

A ^{210}Pb – ^{226}Ra – ^{230}Th – ^{238}U study of Klyuchevskoy and Bezymianny volcanoes, Kamchatka

Simon Turner ^{a,*}, Kenneth W.W. Sims ^b, Mark Reagan ^c, Craig Cook ^d

^a GEMOC, Department of Earth & Planetary Sciences, Macquarie University, Australia

^b Department of Geology & Geophysics, Woods Hole Oceanographic Institution, USA

^c Department of Geoscience, University of Iowa, USA

^d School of Science and Engineering, University of Waikato, Private bag 3105, Hamilton, New Zealand

Received 30 January 2007; accepted in revised form 7 August 2007; available online 7 September 2007

Abstract

Lavas from Klyuchevskoy and Bezymianny volcanoes, Kamchatka, appear to show a link between the extent of partial melting in their mantle source region and the subsequent degree of fractionation suffered by the magmas during passage through the crust. This fractionation may have occurred on timescales significantly less than 1000 years if observed ^{226}Ra excesses largely reflect variable residual porosity in the source melting region. Unlike most arc lavas, those with the highest MgO contents and Ba/Th ratios have the lowest ^{226}Ra excess. Forward models suggest that those portions of the source which had undergone the greatest addition of U by fluids from the subducting plate also underwent the greatest extents of partial melting at the highest residual porosity. At Klyuchevskoy, a change from eruption of high-MgO to high- Al_2O_3 basaltic andesites around 1945 is reflected in an increase in size of ^{226}Ra excess which seems to require a simultaneous decrease in residual porosity and suggests a rapid changes in the melting regime. The eruption of andesites at Bezymianny, simultaneous with the eruption of basaltic andesites at Klyuchevskoy, further suggests that different degree melts produced at differing residual porosity can be formed and extracted from the melt region at the same time. Thus, the melting processes beneath Klyuchevskoy and Bezymianny are demonstrably complex. They have clearly been influenced by both fluid addition from the subducting plate and extension and decompression beneath the Central Kamchatka Depression. Finally, the ^{210}Pb data are, with one or two exceptions, in equilibrium with ^{226}Ra , suggesting that there was restricted relative magma-gas movement in this highly productive magmatic system.

© 2007 Elsevier Ltd. All rights reserved.

1. INTRODUCTION

Over the past decade, U-series disequilibria have provided a number of important insights into the physical processes of melt generation and magma evolution at subduction zones though, in general, these insights derive from depleted oceanic arcs where the observations are most extreme (see Turner et al., 2003, for a recent review). In comparison, investigations of continental arcs are fewer in number and frequently compromised by a lack of primitive lavas which should, in principle, most closely preserve the

least modified mantle signature. With a limited knowledge of the primitive lavas, the assessment of signatures in more evolved lavas can prove problematic. Second, although U-series data can also be used to constrain magma differentiation time scales (see Hawkesworth et al., 2004, for a recent review), they have not yet been applied to the debate over whether high- Al_2O_3 basalts result from differentiation of high-MgO basalt parents (e.g. Nichols and Ringwood, 1973; Crawford et al., 1987), partial melting of subducted basalt followed by reaction with the mantle wedge (e.g. Brophy and Marsh, 1986; Kelemen, 1990) or plagioclase accumulation (e.g. Fournelle and Marsh, 1991). Third, recent studies have highlighted the potential of the ^{210}Pb – ^{226}Ra system to provide information on magma degassing (e.g. Gauthier and Condomines, 1999; Berlo et al.,

* Corresponding author. Fax: +61 2 9850 8943.

E-mail address: sturner@els.mq.edu.au (S. Turner).

2004; Reagan et al., 2006). However, these have largely focussed on volcanoes at which there has been little recent variation in lava composition and, even though a recent global survey has hinted at a possible correlation between ($^{210}\text{Pb}/^{226}\text{Ra}$) and SiO_2 , which might inform models for volcanic hazards (Turner et al., 2004), no study has yet been conducted to see whether a similar trend occurs within a single volcanic system. Lavas erupted during the last century from Klyuchevskoy and associated Bezyminany volcano in Kamchatka afford the opportunity to address all three of these issues.

2. GEOLOGICAL SETTING AND SAMPLE DETAILS

Kamchatka lies between two oceanic island arc systems in the north Pacific formed by subduction of Mesozoic Pacific oceanic crust beneath the Eurasian plate to the west (Kurile-arc) and the North American plate to the north (Aleutian arc). The junction with the Aleutian arc divides the Kamchatka Peninsula into northern and central segments and the Petropavlovsk fault zone separates the southern and central segments (Fig. 1). The southern segment has a Kurile-type volcanic basement whereas the central and northern segments have 30–40 km thick crust

formed from accreted Mesozoic and Tertiary oceanic and island arc terranes (e.g. Geist et al., 1994). Intra-arc extension has resulted in a large graben oriented parallel to the trench ~ 200 km above the Benioff zone known as the Central Kamchatka Depression (CKD). The CKD separates the Eastern Volcanic Front (EVF) from the rear arc volcanic zone of the Sredinny Ridge, which is now largely inactive. The northern segment was formed by westward subduction of newly formed oceanic crust produced by short-lived spreading in the Komandorsky Basin but volcanism ceased here around 2 Ma (Baranov et al., 1991). Subduction is orthogonal to the arc at $\sim 9 \text{ cm a}^{-1}$ and the Benioff zone dips at $40^\circ\text{--}50^\circ$ reaching depths of $\sim 170\text{--}220$ km beneath the EVF and $\sim 200\text{--}260$ km beneath the CKD (Kepezhinskas et al., 1997 and references therein).

Lavas from Kamchatka are largely tholeiitic to calc-alkaline and often highly magnesian. Some more K-rich lavas do occur, particularly in the northern segment along with adakites and Nb-rich lavas which may reflect slab melts of the newly subducted, hot oceanic crust formed in the Komandorsky Basin (Hochstaedter et al., 1996; Kepezhinskas et al., 1997). Of the active southern segment volcanoes, Hochstaedter et al. (1996) presented evidence that lavas from the CKD have higher Ce/Yb ratios compared

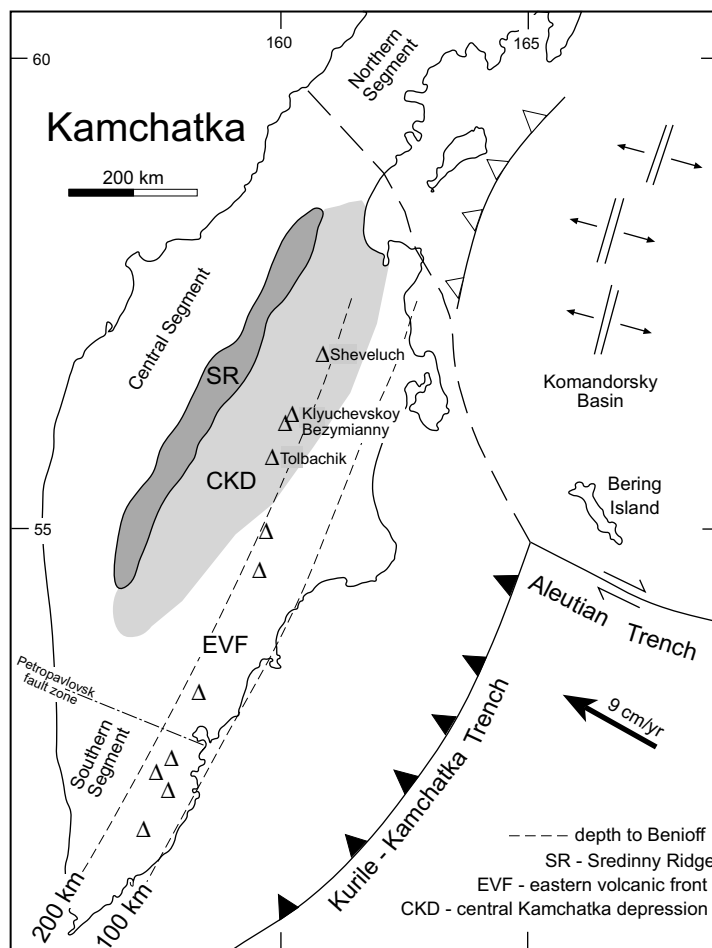


Fig. 1. Map of Kamchatka showing the location of Klyuchevskoy and Bezymianny volcanoes in relation to the arc-front volcanoes.

to those from the EVF lavas and argued that this reflects depletion of the mantle wedge beneath the CKD as it convects from the rear towards the EVF. Sr, Nd, and Pb isotopes are generally very similar to Pacific MORB suggesting a relatively minor contributing role for the subducted sediments (Kersting and Arculus, 1995; Kepezhnikas et al., 1997). Turner et al. (1998) conducted a regional U–Th study of lavas from the EVF and CKD concluding that the integrated age of U addition by fluids was ~150 kya.

Klyuchevskoy volcano forms part of the Klyuchevskaya group of volcanoes and is located in the northern CKD with Bezymianny lying on its flank some 20 km to the south (Fig. 1). Klyuchevskoy is dominated by high-MgO basalt and high-Al₂O₃ basaltic andesite lavas flows and pyroclastic deposits and is the most active arc volcano in the world with a mean eruption rate over the last 10 kyr of ~1 m³/s (Fedotov et al., 1987), equivalent to a 50 km segment of mid-ocean ridge. In a detailed study, Kersting and Arculus (1994) invoked a model involving recharge, tapping and fractionation (RTF) to explain the genesis of the high-Al₂O₃ basaltic andesites from high-MgO parental magmas. Ozerov (2000) came to the same conclusion in a study of mineral inclusions and Ariskin et al. (1995) have related the two series by polybaric fractionation under hydrous conditions. Pb isotope ratios of Klyuchevskoy lavas show no shift from the Pacific MORB field to more radiogenic values precluding the addition of even quite small amounts of sediment to their source (Kersting and Arculus, 1995). The latest eruptive cycle at Bezymianny volcano commenced in 1955 with a sector-collapse triggered eruption in 1956. This volcano has largely erupted andesitic products and Ozerov et al. (1997) argued that these have a close genetic relationship to the Klyuchevskoy basaltic andesites suggesting that lavas from the two volcanoes in fact belong to a single evolutionary series. In a U-series study of the Klyuchevskaya group of volcanoes, Dosseto et al. (2003) argued that two end-member mixing dominated the system. High-MgO basalts from Klyuchevskoy, having large ²²⁶Ra and ²³⁸U excesses, formed one end-member reflecting flux melting of the mantle wedge. In contrast, andesites from Bezymianny, that have ²³⁰Th and ²³¹Pa excesses coupled with near-equilibrium (²²⁶Ra/²³⁰Th), were inferred to be dominated by a slab-melt component. Here, we present new data from Klyuchevskoy including 3 high-MgO basalts erupted between 1900 and 1938 and 9 high-Al₂O₃ basaltic andesites erupted between 1945 and 1993 along with data from 9 andesites erupted from Bezymianny between 1950 and 1991 in order to address their origin and petrogenesis.

3. ANALYTICAL TECHNIQUES

Major element data come from Ozerov et al. (1997) whereas trace element data (with relative errors of ~5–10%) were obtained by ICP-MS at Washington State University (Knaack et al., 1994). Nd and Sr isotope data for 8 representative samples were measured at WHOI by MC-ICP-MS using a ThermoFinnigan Neptune (Table 2). Data are reported relative to 0.71024 (NBS 987) and 0.511847 (La Jolla), respectively. Based upon replicate analysis of

the NBS SRM 987 and La Jolla Nd isotopic standards, two sigma precisions for Sr and Nd isotope data are less than ±30 ppm and less than ±20 ppm, respectively.

U, Th, and Ra concentrations and isotope ratios were determined on samples that were spiked with ²³⁶U–²²⁹Th and ²²⁸Ra tracers and dissolved using an HF–HNO₃–HCl mix in heated teflon pressure bombs. The product was converted to chloride using 6 N HCl and then 6 N HCl saturated with H₃BO₃ to remove residual fluorides. The final product was converted to nitrate using 14 N HNO₃ and finally taken up in 7 N HNO₃. U and Th purification was achieved via a single pass through a 4 ml anionic resin column using 7 N HNO₃, 6 N HCl and 0.2 N HNO₃ as eluents. Concentrations and isotope ratios were measured in dynamic mode on a Nu Instruments® MC-ICP-MS at Macquarie University. ²³⁸U and ²³⁵U were analysed on Faraday cups, using the ²³⁸U/²³⁵U ratio to determine the mass bias, assuming ²³⁸U/²³⁵U = 137.88, whilst ²³⁶U and ²³⁴U were alternately collected in the IC0 ion counter which is equipped with a deceleration lens. The IC0 gain was determined during interspersed dynamic analyses of CRM145 assuming a ²³⁴U/²³⁸U ratio of 5.286 × 10⁻⁵ (Cheng et al., 2000). Th isotopes were also measured dynamically with ²³²Th in Faraday cups and ²³⁰Th and ²²⁹Th alternating on IC0. The mass bias and gain for these measurements was taken in the first instance from measurements of CRM145. Differences in the mass bias for U and Th were then determined by interspersed analyses of the Th‘U’ solution standard. Accuracy (<0.3%) and precision (<0.1%) were assessed by regular analyses of the U010 and ThA solution standards (see Dosseto et al., 2006). Analysis of the secular equilibrium rock standard TML-3 performed at the same time as the samples yielded the following results: U = 10.54 ppm, Th = 29.61 ppm, (²³⁴U/²³⁸U) = 0.993, (²³⁰Th/²³²Th) = 1.088, (²³⁰Th/²³⁸U) = 1.007. U–Th measurements were also replicated, within analytical uncertainties (excepting the U concentration for B00001), for 8 samples at WHOI (Table 2) using methods described in the Appendix.

The Ra procedure followed that described in Turner et al. (2000). Ra was taken from the first elution from the anionic column and converted to chloride using 6 N HCl. This was then loaded in 3 N HCl onto an 8 ml cationic column and eluted using 3.75 M HNO₃ and the process repeated on a scaled-down 0.6 ml column. Ra and Ba were then chromatographically separated using ElChrom® Sr-spec resin™ and 3 N HNO₃ as elutant in a 150 µl procedure. Samples were loaded onto degassed Re filaments using a Ta–HF–H₃PO₄ activator solution (Birck, 1986) and ²²⁸Ra/²²⁶Ra ratios were measured to a precision typically ~0.5% in dynamic ion counting mode on a ThermoFinnigan Triton® TIMS at Macquarie University. Accuracy was assessed via replicate analyses of TML-3 that yielded ²²⁶Ra = 3534 fg/g and (²²⁶Ra/²³⁰Th) = 1.002 ± 0.008 (n = 5). Ra measurements were also replicated (assuming secular equilibrium between ²¹⁴Pb and ²²⁶Ra), within analytical uncertainties, for 8 samples at WHOI (Table 2) using γ-spectroscopy methods described in the Appendix.

²¹⁰Pb procedures are based on those of Reagan et al. (2005) and assume secular equilibrium between ²¹⁰Pb and

^{210}Po , ^{210}Po concentrations were determined from measurements on separate 2g sample dissolutions which were spiked with a ^{209}Po tracer calibrated against a value of 7.95 dpm/g for TML-2 (Reagan et al., 2005). Samples were loaded onto a 1 ml anionic column in 1 N HCl containing H_3BO_3 where most major and trace elements were washed off in 1 N and 0.5 N HCl after which Po was eluted in warm 7.5 N HNO_3 . Po was auto-plated onto Ag discs above a magnetic stirrer for 6–8 h in 150 ml of warm 0.5 N HCl which contained ascorbic acid. ^{210}Po and ^{209}Po were counted for approximately a week using an α -counting system at the University of Iowa. Many of the samples were analysed multiple times to check reproducibility (Table 3). The errors on $(^{210}\text{Pb}/^{226}\text{Ra})_0$ are dominated by the analytical error on ^{210}Po and this is significantly magnified by the extrapolation to eruption age in those samples which are older than one half life (22.6 yrs). Activity ratios (denoted by brackets) for all U-series data were calculated using the half-lives compiled in Bourdon et al. (2003).

4. RESULTS

The three high-MgO basalts from Klyuchevskoy have $\text{SiO}_2 = 51.4\text{--}52.2\%$ and $\text{MgO} = 11.5\text{--}8.1\%$ ($\text{Mg}\# = 0.71\text{--}0.63$) and are porphyritic (7–10 modal%) containing olivine ($\text{Fo}_{92\text{--}87}$) and augite in a microcrystalline groundmass (Ozerov et al., 1997). The high- Al_2O_3 basaltic andesites have $\text{SiO}_2 = 53.5\text{--}53.9\%$ and are distinguished from the high-MgO basalts by their higher total alkalis (Fig. 2a) and their lower MgO and by having $\text{Al}_2\text{O}_3 > 16.5\%$ (Fig. 2b). In addition to olivine and augite, the basaltic andesites also contain plagioclase and orthopyroxene phenocrysts. The Bezymianny andesites have $\text{SiO}_2 = 57.4\text{--}61.0\%$ and $\text{MgO} = 3.9\text{--}2.7\%$ and overlap in total alkalis and Al_2O_3 with the high- Al_2O_3 basaltic andesites (Fig. 2). The phenocryst assemblage in the Bezymianny andesites includes pyroxene, plagioclase and subordinate magnetite and hornblende. Sample B0000, erupted in 1950, belongs to an earlier eruptive sequence than the rest of the Bezymianny andesites analysed here and this sample is distinguished by higher SiO_2 and lower Al_2O_3 (Fig. 2).

Compatible trace element abundances such as Cr and Ni are enriched in the high-MgO basalts (up to 770 and 182 ppm, respectively) and decrease with increasing SiO_2 through the high- Al_2O_3 basaltic andesites to the andesites (Table 1). The exception is sample B0000, which despite having the highest SiO_2 of all the samples analysed, has 112 ppm Cr and 29 ppm Ni, significantly greater than the other andesites. Primitive mantle-normalised incompatible trace element patterns are typical of arc lavas in so much as fluid-mobile elements (Ba, U, K, Pb, and Sr) are enriched and Th, Nb, and Ti are depleted relative to the rare earth elements (Fig. 3). The rare earth element patterns are fairly flat with the exception of sample B0000 which is strongly depleted in heavy rare earth elements compared to the other lavas (Fig. 3) and this sample also has $\text{Sr}/\text{Y} = 43$ which contrasts strongly with the other lavas ($\text{Sr}/\text{Y} = 13\text{--}18$).

The Nd and Sr isotope ratios of the Klyuchevskoy basalts and Bezymianny andesites measured in this study range from 0.513097 to 0.513117 and 0.70345 to 0.70353, respec-

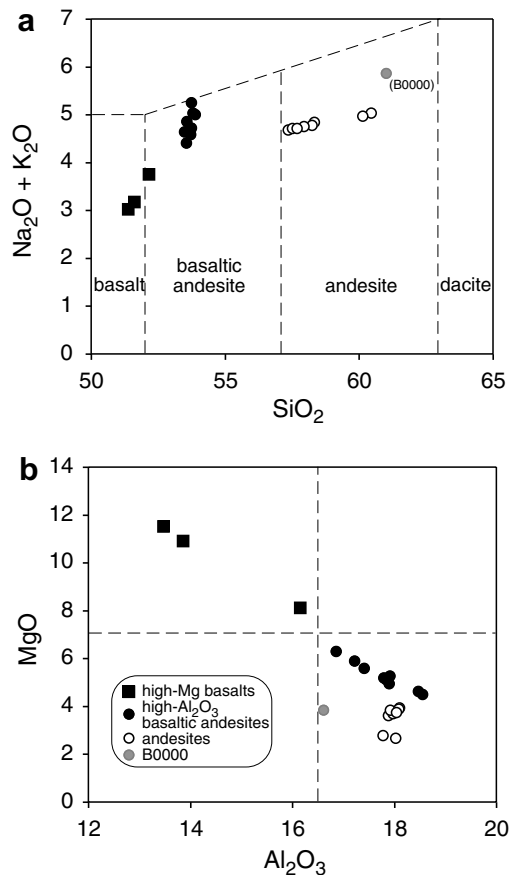


Fig. 2. Plots of (a) $\text{Na}_2\text{O} + \text{K}_2\text{O}$ versus SiO_2 and (b) MgO versus Al_2O_3 showing the broad compositional range of the lavas (high-MgO basalts = filled squares; high- Al_2O_3 basaltic andesites = filled circles; andesites = open circles; sample B0000 = grey circle). Delineation of the high-MgO and high- Al_2O_3 basaltic andesite fields from Crawford et al. (1987).

tively (Table 2). These data are essentially the same, within analytical uncertainties, of those reported previously by Ozerov et al. (1997) and Kersting and Arculus (1995). The limited isotopic range of the samples suggest that these rocks come from a source which is homogeneous over the length scale of melting and that these lavas can be treated as cogenetic when considering their petrogenesis.

The U-series data show that all samples have $(^{234}\text{U}/^{238}\text{U})$ within analytical error ($\sim 1\%$) of secular equilibrium. Consistent with other published data from Kamchatka (Turner et al., 1998; Dosseto et al., 2003), the lavas also have high $(^{238}\text{U}/^{232}\text{Th})$ ratios and the new data extend the range further (Fig. 4a). All of the lavas have U excesses with $(^{230}\text{Th}/^{238}\text{U}) = 0.89\text{--}0.97$ and so these samples show some differences from those analysed by Dosseto et al. (2003) in that their Bezymianny andesites and some of their high- Al_2O_3 basaltic andesites from Klyuchevskoy had Th excesses. Again, sample B0000 is an exception within our data, having a $(^{230}\text{Th}/^{238}\text{U})$ ratio of 0.76. Fig. 4b shows that $(^{226}\text{Ra}/^{230}\text{Th})$ is highest in the high- Al_2O_3 basaltic andesites (1.49–1.69) and lower in the andesites (1.28–1.34). This is broadly similar to the data presented by Dos-

Table 1
Analyses of recent Klyuchevskoy and Bezymianny lavas

Sample No.	K0012	K0032	K1938	K1945	K1946	K1951	K1953	K1956	K1966	K1983	K1988	K1993	B0000	B1956-1	B1977	B1981	B1986	B1987	B1989-1	B1990	B1991
Eruption year	1900	1910	1938	1945	1946	1951	1953	1956	1966	1983	1988	1993	1950	1956	1977	1981	1986	1987	1989	1990	1991
SiO ₂ (wt%)	51.39	52.16	51.62	53.55	53.70	53.57	53.89	53.80	53.71	53.74	53.48	53.74	61.01	60.45	58.33	58.25	57.95	60.14	57.35	57.52	57.68
TiO ₂	0.80	0.90	0.82	1.01	1.06	1.10	1.11	1.12	1.05	1.10	1.11	1.08	0.54	0.57	0.69	0.69	0.71	0.59	0.72	0.73	0.71
Al ₂ O ₃	13.48	16.16	13.86	16.86	17.41	17.91	18.47	18.55	17.22	17.79	17.84	17.90	16.62	17.78	17.88	17.97	17.92	18.03	18.10	18.09	18.04
Fe ₂ O ₃	9.48	9.49	9.64	9.28	9.25	9.07	9.08	9.06	9.13	9.41	9.58	9.48	5.45	6.35	7.31	7.32	7.43	6.61	7.72	7.66	7.63
MnO	0.17	0.16	0.17	0.16	0.17	0.15	0.15	0.15	0.16	0.16	0.17	0.17	0.10	0.14	0.14	0.14	0.14	0.15	0.15	0.15	0.15
MgO	11.51	8.11	10.90	6.29	5.58	5.27	4.63	4.50	5.89	5.18	5.12	4.94	3.82	2.77	3.61	3.70	3.83	2.67	3.93	3.88	3.74
CaO	10.21	9.54	10.11	8.73	8.47	8.14	7.97	8.01	8.61	8.35	8.40	8.21	6.04	6.47	7.19	7.29	7.33	6.64	7.50	7.42	7.39
Na ₂ O	2.47	3.09	2.58	3.35	3.53	3.67	3.80	3.84	3.51	3.55	3.58	3.64	4.56	3.72	3.63	3.58	3.56	3.69	3.51	3.53	3.52
K ₂ O	0.55	0.66	0.59	1.06	1.11	1.19	1.20	1.19	1.07	1.07	1.06	1.08	1.31	1.31	1.21	1.20	1.19	1.28	1.17	1.18	1.19
P ₂ O ₅	0.12	0.13	0.12	0.19	0.20	0.21	0.21	0.21	0.19	0.19	0.19	0.19	0.16	0.17	0.16	0.16	0.16	0.18	0.16	0.16	0.16
LOI	0.04	-0.26	-0.31	-0.59	-0.34	-0.37	-0.43	-0.33	-0.36	-0.37	-0.47	-0.24	0.32	0.19	0.01	-0.12	-0.03	-0.04	-0.12	-0.13	-0.01
Total	100.22	100.14	100.10	99.89	100.14	99.91	100.08	100.10	100.18	100.80	100.06	100.19	99.93	99.92	100.16	100.18	100.19	99.94	100.19	100.19	100.20
Sc (ppm)	37.7	32.9	36.9	30.4	28.92	24.38	23.93	23.91	29.01	27.25	27.93	26.75	14.36	13.8	18.78	19.35	19.84	12.97	20.87	20.48	20.04
V	242	250	245	237	236	245	235	229	245	264	275	250	102	96	129	134	144	87	141	138	137
Cr	770	267	757	100	55	49	20	19	104	43	27	29	112	15	23	24	21	12	21	18	18
Ni	182	78	170	39	26	30	21	21	36	24	23	25	29	8	14	10	14	7	15	12	12
Cu	64	83	84	105	113	110	118	120	99	99	101	94	26	12	63	31	35	13	42	38	41
Zn	71	85	76	74	77	83	77	76	82	85	86	84	53	72	64	65	63	72	69	61	62
Ga	16	18	14	19	19	20	19	21	18	19	19	19	17	16	17	17	17	18	17	20	19
As	1.4	1.1	1	1.5	0.9	1.5	1.7	1	0	2.2	1.7	2.2	6.6	2.8	2.2	3	2.6	1.8	2.2	2	2.5
Se	0	0	0	0	0	0	1	0	0				0.8	0	0	0	0	0			
Br	0	1.2	0	0.8	1	0.7	0.9	0.4	0	0	1	1.2	1	0.8	1	1	1	0	0	0.8	0.8
Rb	9.3	11.2	9.4	16.5	16.9	19	18	19.6	17.5	17.6	17.7	18.2	23	25	23	22	22	24	21	22	22
Sr	255	328	263	390	403	411	420	424	375	378	380	377	561	355	350	348	344	360	348	350	350
Y	19	21	20	24	25	24	25	26	25	27	26	26	13	20	22	22	21	20	21	21	20
Zr	67	77	67	94	98	104	104	103	98	104	101	103	108	116	107	106	104	113	102	102	103
Nb	1.5	1.7	0.9	2.8	2	1.9	1.2	2.6	2.5	2.2	2.8	1.8	3	4	4	4	4	4	4	4	4
Sb	0.1	0.2	0.1	0.2	0.2	0.2	0.2	0.2	0.2	0.2	0.2	0.2	0.6	0.3	0.3	0.2	0.3	0.2	0.2	0.2	0.2
Cs	0.31	0.27	0.3	0.48	0.49	0.55	0.57	0.55	0.52	0.55	0.48	0.49	0.9	0.96	0.82	0.84	0.8	0.89	0.77	0.82	0.85
Ba	243	234	237	394	401	429	445	434	407	428	433	430	397	464	426	408	405	402	385	385	375
La	4.04	4.97	4.28	6.6	6.93	7.49	7.47	7.37	6.98	7.31	7.1	7.37	7.81	9.15	8.47	8.27	8.1	9.13	8.12	8.08	8.42
Ce	11	13.3	10.9	17.1	17.5	18.5	18.5	17.97	17.5	17.6	17.4	17.3	18.5	20.9	19.2	19.7	19.3	21	18.5	18.6	19
Nd	0	0	8.4	12.6	13.6	0	0	12.5	14.1	12.6	0	12.2	9.6	10.7	0	0	0	12.3	11.7	0	0
Sm	2.55	2.76	2.61	3.35	3.52	3.63	3.73	3.76	3.57	3.74	3.69	3.73	2.66	3.19	3.13	3.13	3.13	3.21	3.08	3.1	3.08
Eu	0.831	0.956	0.868	1.104	1.136	1.171	1.18	1.203	1.158	1.181	1.192	1.181	0.81	1	0.99	1.01	0.98	1.02	0.97	0.96	0.97
Tb	0.46	0.5	0.5	0.58	0.63	0.63	0.65	0.62	0.61	0.66	0.64	0.64	0.35	0.52	0.5	0.53	0.54	0.5	0.53	0.51	0.48
Yb	1.75	1.87	1.92	1.99	2.06	2.17	2.32	2.24	2.29	2.35	2.38	2.41	1.22	2.04	1.99	2	1.98	1.99	1.93	2.07	1.94
Lu	0.251	0.246	0.254	0.271	0.293	0.337	0.334	0.336	0.321	0.349	0.34	0.372	0.16	0.27	0.304	0.285	0.293	0.307	0.287	0.281	0.289
Hf	1.82	2	1.97	2.5	2.64	2.86	2.77	2.82	2.67	2.8	2.68	2.68	2.94	3.12	2.87	2.87	2.75	3.2	2.75	2.69	2.75
Pb	2.3	2.8	5.6	3.3	4.2	3.8	5.9	5.4	5.1	4.7	5.1	4.4	5	5	6	5	6	7	4	4	5
Th	0.367	0.450	0.396	0.682	0.684	0.727	0.734	0.737	0.683	0.747	0.704	0.755	1.071	1.270	1.160	1.143	1.093	1.208	1.056	1.085	1.079

(continued on next page)

Table 1 (continued)

Sample No.	K0012	K0032	K1938	K1945	K1946	K1951	K1953	K1956	K1966	K1983	K1988	K1993	B0000	B1956-1	B1977	B1981	B1986	B1987	B1989-1	B1990	B1991
Eruption year	1900	1910	1938	1945	1946	1951	1953	1956	1966	1983	1988	1993	1950	1956	1977	1981	1986	1987	1989	1990	1991
U	0.264	0.312	0.283	0.449	0.453	0.487	0.492	0.497	0.460	0.475	0.462	0.482	0.727	0.885	0.804	0.792	0.781	0.848	0.752	0.758	0.767
²²⁶ Ra (dpm/g)	0.223	0.279	0.245	0.554	0.577	0.618	0.626	0.560	0.546	0.573	0.586	0.562	0.689	0.855	0.776	0.764	0.753	0.817	0.745	0.745	0.750
(²³⁴ U/ ²³⁸ U)	1.009	1.009	1.010	1.008	1.009	1.011	1.006	1.007	1.005	0.992	1.006	0.998	0.983	1.011	1.014	1.009	1.005	1.001	1.000	1.003	1.008
(²³⁸ U/ ²³² Th)	2.184	2.103	2.166	1.995	2.009	2.032	2.034	2.043	2.042	1.929	1.990	1.939	2.058	2.115	2.103	2.101	2.166	2.131	2.160	2.120	2.158
(²³⁰ Th/ ²³² Th)	1.950	1.965	1.957	1.930	1.943	1.959	1.979	1.955	1.926	1.864	1.880	1.862	1.554	2.022	2.011	1.953	2.047	2.036	2.013	2.006	2.033
(²³⁰ Th/ ²³⁸ U)	0.893	0.934	0.903	0.967	0.967	0.964	0.973	0.957	0.943	0.966	0.944	0.960	0.755	0.956	0.956	0.929	0.945	0.955	0.932	0.946	0.942
(²²⁶ Ra/ ²³⁰ Th)	1.202	1.239	1.232	1.643	1.681	1.677	1.694	1.517	1.583	1.632	1.712	1.584	1.626	1.310	1.312	1.325	1.327	1.298	1.363	1.346	1.335

seto et al. (2003), although our (²²⁶Ra/²³⁰Th) ratios are generally lower and have a more restricted range within each lava group, although sample B0000 is an exception with (²²⁶Ra/²³⁰Th) = 1.60. Globally, the highest (²²⁶Ra/²³⁰Th) ratios tend to be observed in the most mafic lavas (Turner et al., 2003) and this is also true of the Klyuchevskoy and Bezymianny data presented by Dosseto et al. (2003). Thus, it is significant that we find that the (²²⁶Ra/²³⁰Th) ratios are lowest in the high-MgO basalts (1.18–1.22) (Fig. 4b) and this was reproduced by γ -spectrometry at WHOI. Dosseto et al. (2003) also presented data on high-MgO and high-Al₂O₃ basalts from nearby Tolbachik volcano and these are also compared with data on similar rocks published by Turner et al. (1998, 2001) on Fig. 4. The high-MgO basalt samples analysed by both groups have ²³⁸U excesses and sizeable ²²⁶Ra excesses and are thus much more typical of primitive basalts worldwide than the unusual signature found here in the Klyuchevskoy high-MgO basalts. In contrast, two high-Al₂O₃ basalts analysed from Tolbachik by Dosseto have ²³⁰Th excesses.

In summary, our new U–Th–Ra data show some important differences to that of Dosseto et al. (2003) but we have obtained good reproducibility between the Macquarie and WHOI laboratories and the different rock types show good internal consistency with the exception of B0000 which has somewhat lower Yb than the other lavas. The origin of the U-series differences is not yet clear but will be investigated further elsewhere (Dosseto pers. comm.).

The first ²¹⁰Pb data from Klyuchevskoy and Bezymianny are presented in Table 3. When the (²¹⁰Pb/²²⁶Ra) ratios and their errors are propagated to their eruption age, only two samples have ²¹⁰Pb–²²⁶Ra disequilibria outside of 2 σ analytical error. Three analyses of high-Al₂O₃ basaltic andesite (K1945) have a ²¹⁰Pb excesses, although only one is outside of secular equilibrium in terms of 2 σ analytical error (see Table 3). However, this sample is the first basaltic andesite that erupted from Klyuchevskoy after several decades of eruption of high-Mg basalt. In contrast, sample K1951 has a ²¹⁰Pb deficit just outside of 2 σ analytical error.

5. DISCUSSION

5.1. Partial melting and fractionation models

On the basis of their Mg#’s and forsteritic olivines, two of the three high-MgO basalts appear to be near primary melts unmodified from the mantle, the other is more fractionated. The high-Al₂O₃ basaltic andesites are more evolved with lower Mg#s and could reflect fractionation from parental magmas similar to the high-MgO basalts (Kersting and Arculus, 1994; Ozerov, 2000). The Bezymianny andesites are the most evolved lavas but do not lie on an extrapolation of trends defined by the high-MgO and high-Al₂O₃ basaltic andesites on many bivariate diagrams (e.g. Figs. 2a and b) precluding simple petrogenetic models involving fractionation from the basalts. Furthermore, although the most incompatible element concentrations (e.g. Rb, Th) increase from high-MgO basalt through high-Al₂O₃ basaltic andesite to andesite (Fig. 3), the same is not true of the less incompatible elements and the pat-

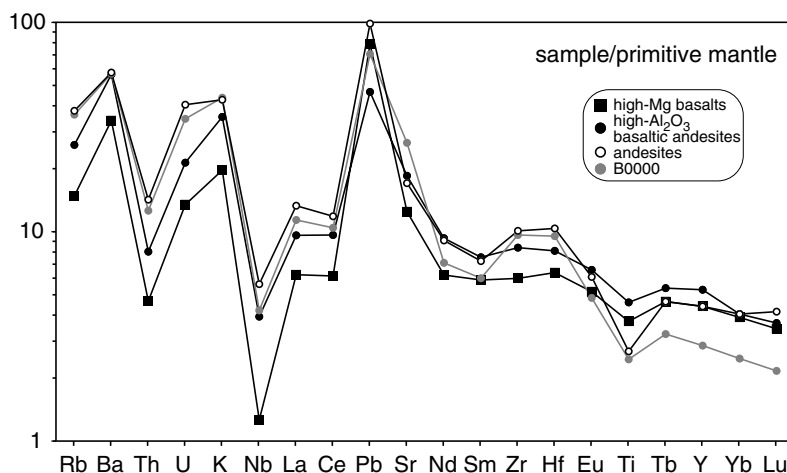


Fig. 3. Primitive mantle-normalised incompatible element diagram for a representative lava from each of the three groups plus B0000.

Table 2

Sr and Nd isotope data and U–Th–Ra measurements performed at WHOI

Sample No.	Th (ppm)	U (ppm)	$(^{238}\text{U}/^{232}\text{Th})$	$(^{230}\text{Th}/^{232}\text{Th})$	^{226}Ra (dpm/g)*	$^{87}\text{Sr}/^{86}\text{Sr}$	$^{143}\text{Nd}/^{144}\text{Nd}$
K0012	0.341	0.243	2.165	1.952	0.241	0.703453	0.513112
K0032	0.452	0.310	2.080	1.968	0.270	0.703521	0.513097
K1938	—	—	—	—	0.252	—	—
K1945	0.684	0.451	2.001	1.932	0.540	0.703531	0.513113
K1946	—	—	—	—	0.578	—	—
K1953	0.736	0.490	2.020	1.984	—	0.703491	0.513099
K1983	0.742	0.476	1.945	1.879	—	0.703483	0.513107
K1988	—	—	—	—	0.580	—	—
B0000	1.075	0.629	1.775	1.541	0.674	0.703452	0.513108
B1977	1.158	0.806	2.111	2.020	—	0.703519	0.513117
B1987	—	—	—	—	0.809	—	—
B1989-1	1.196	0.852	2.162	2.015	—	0.703482	0.513116

* Based on ^{214}Pb γ -counting data.

terns are pegged at Yb. This not only further precludes the andesites from being fractionated equivalents of the high- Al_2O_3 basaltic andesites but also casts doubt on models relating the high-MgO and high- Al_2O_3 basaltic andesites by fractional crystallisation (e.g. Kersting and Arculus, 1994). Finally, if simple fractionation models were applicable to these Klyuchevskoy and Bezymianny lavas, ratios of incompatible elements should be more or less constant in all three lava suites. However, Fig. 5 shows that although Th/Hf ratios are constant within each lava suite they vary between the suites.

The observation that Th/Hf varies between suite but remains constant within a given suite suggests that the three lava suites each evolved from different parental magmas. Conversely, the similarities of their Nd and Sr isotopic compositions (Table 2) and incompatible trace element patterns on Fig. 3 suggest they had a similar mantle source composition. One way to reconcile these apparently disparate observations is that the different parental magmas reflect differing extents of partial melting of a homogeneous source. This is suggested by the rotation of incompatible

trace element patterns on Fig. 3. The plot of Th/Hf versus Th in Fig. 6 is a process identification diagram (e.g. Allegre and Minster, 1978) on which partial melting forms a steep vector whereas fractionation leads to a near horizontal trend. The data form a steep trend on Fig. 6 and similar diagrams such as Nb/Zr versus Nb (not shown). On Fig. 6, a model partial melting vector of a nominal mantle source was constructed so as to pass near the high-MgO basalts, which are inferred to be near primary melts. The high- Al_2O_3 basaltic andesites and andesites have higher Th/Hf and lie to the right of the partial melting vector (see Fig. 6). Thus, they can be modelled to reflect increasing degrees of fractionation from magmas derived from progressively smaller extents of partial melting. Although the model shown on Fig. 6 is non-unique, the extent of partial melting implied for the parental magmas decreases from 30% for the high-MgO basalts, to ~20% for the high- Al_2O_3 basaltic andesites to <15% for the andesites. The marked difference in Ba/Th ratio between the basalts (519–662) and andesites (332–370) also argues for derivation from different magma batches. The degree of fraction-

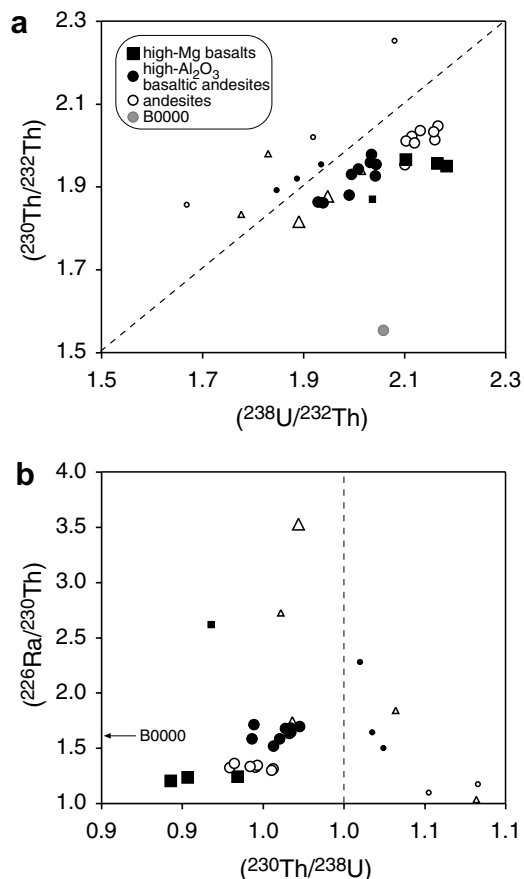


Fig. 4. (a) $(^{230}\text{Th}/^{232}\text{Th})$ versus $(^{238}\text{U}/^{232}\text{Th})$ and (b) $(^{226}\text{Ra}/^{230}\text{Th})$ versus $(^{230}\text{Th}/^{238}\text{U})$ for lavas from Klyuchevskoy and Bezmyanny. Large triangles are data for Tolbachik lavas from Turner et al. (1998). Small symbols are data for equivalent rock types from Dosseto et al. (2003). Sample B0000 plots outside of the field of view in (b).

ation implied for the high- Al_2O_3 basaltic andesites (20–30%) is similar to that estimated by Kersting and Arculus (1994) for similar samples and the model suggests reasonable extents of fractionation for the andesites (30–45%).

5.2. Constraints on melting processes and fractionation time scales from ^{226}Ra – ^{230}Th – ^{238}U disequilibria

One of the objectives of this study is to combine the simple petrogenetic model developed above with the ^{226}Ra – ^{230}Th – ^{238}U disequilibria in order to constrain the time scales and mechanisms of fluid addition, partial melting and magma differentiation. The occurrence of U and Ra excesses in all of the lavas is consistent with fluid addition of these mobile elements to the mantle wedge from the subducting Pacific plate (see Turner et al., 2003 for a recent review). Fig. 7a shows that lavas analysed for Pb isotopes from Klyuchevskoy and Tolbachik volcano have lower K_{Th} than MORB but similar radiogenic Pb implying that their source underwent a recent lowering of Th/U, consistent with recent addition of U. The broadly positive correlation between $(^{226}\text{Ra}/^{230}\text{Th})$ and Ba/Th for the high- Al_2O_3

basaltic andesites and andesites (Fig. 7b) is also consistent with the Ra excesses reflecting fluid addition and the same relationship was found by Dosseto et al. (2003). Fig. 7c also shows that $(^{226}\text{Ra}/^{230}\text{Th})$ decreases with decreasing MgO from the high- Al_2O_3 basaltic andesites to the andesites, which could be consistent with fractionation over a few 1000 yrs. However, these two trends are not continued through to the high-MgO basalts and an important issue is why these latter rocks do not have the highest ^{226}Ra excesses. The corollary is that, since the U-series disequilibria in the high-MgO basalts is likely to be primary, the high- Al_2O_3 basaltic andesites and andesites must have evolved from different parental magmas, consistent with the arguments based on Fig. 6.

Since both fluid addition and partial melting are likely causes of U-series disequilibria in arc lavas (see Turner et al., 2003 for a recent review), we have explored dynamic partial melting models simulating partial melting of variably metasomatised mantle sources (Figs. 8–11). The initial source was assumed to be in secular equilibrium chosen to have a $(^{230}\text{Th}/^{232}\text{Th})$ ratio of 1.8 based on the lower bound of values observed for Tolbachik and Klyuchevskoy (Fig. 4). However, since dynamic melting primarily leads to increases in $(^{230}\text{Th}/^{232}\text{Th})$, the large range of U/Th ratios in the lavas requires a broadly equivalent range in U/Th ratios in the source. The effect of metasomatism was modelled by addition of a number of different increments of 0.02 ppm U and the concomitant equilibrium amount of ^{226}Ra resulting in four different hypothetical source compositions (see Fig. 8). Dynamic melting of these four compositions in spinel peridotite facies used the formulation of Williams and Gill (1989), the source mode from Fig. 6 and other parameters listed on Fig. 8a. Following Turner et al. (2006), the melting rate was initially chosen to equate to matrix flowing through the melting zone at 9 cm per yr which is the same as rate of subduction beneath Kamchatka and may thus approximate the rate of convection in the mantle wedge. Generally similar results could be obtained using models that simulate continuous fluid addition and dynamic melting (e.g. Thomas et al., 2002).

It can be seen on Fig. 8a, that dynamic melting of a variably metasomatised peridotite source results in only a gently inclined array which is much shallower than that formed by most of the data. As shown by Turner et al. (1998) and Dosseto et al. (2003), the high $(^{230}\text{Th}/^{232}\text{Th})$ ratios can be explained if a time lag of ~ 150 kyr occurred between fluid addition of U and partial melting and eruption. If this time lag inferred from U–Th disequilibria is correct, then the Ra excesses require a two-stage fluid addition model (e.g. Turner et al., 2000; Dosseto et al., 2003). Dosseto et al. (2003) argued that a continuous fluid addition model (e.g. Thomas et al., 2002) was not able to replicate their Kamchatka data. The alternative, which we have chosen to explore further, is that the Ra excesses predominantly reflect the partial melting process. The U-series signature of most arc lavas are dominated by the effects of fluid addition but ^{231}Pa data require in-growth during partial melting (Turner et al., 2006). Peate et al. (2001) suggested that the relative effect of melting increase across arc and this may be especially relevant to the rear-arc, exten-

Table 3
²¹⁰Po analyses of recent Klyuchevskoy and Bezymianny lavas

Sample No.	²¹⁰ Po (dpm/g)	±1σ	(²¹⁰ Pb/ ²²⁶ Ra)	±1σ	(²¹⁰ Pb) _o	±1σ	(²¹⁰ Pb/ ²²⁶ Ra) _o	±2σ
K0012	0.218	0.011	0.978	0.050	0.102	0.319	0.456	2.861
K0032	0.310	0.011	1.111	0.041	0.833	0.244	2.985	1.747
K0032	0.288	0.011	1.032	0.041	0.440	0.244	1.576	1.746
K1938	0.255	0.015	1.000	0.060	0.255	0.130	1.000	1.022
K1945	0.605	0.028	1.092	0.052	0.865	0.199	1.562	0.720
K1945	0.627	0.017	1.132	0.033	1.000	0.132	1.805	0.478
K1945	0.591	0.016	1.067	0.031	0.780	0.126	1.408	0.455
K1946	0.570	0.019	0.993	0.035	0.550	0.141	0.959	0.491
K1946	0.578	0.020	1.007	0.036	0.598	0.147	1.041	0.512
K1951	0.565	0.018	0.914	0.031	0.349	0.117	0.564	0.378
K1953	0.625	0.021	0.998	0.035	0.621	0.124	0.992	0.397
K1956	0.580	0.018	1.036	0.034	0.647	0.097	1.156	0.348
K1966	0.522	0.017	0.956	0.033	0.469	0.067	0.859	0.244
K1983	0.588	0.031	1.026	0.055	0.602	0.064	1.050	0.225
K1988	0.564	0.021	0.962	0.037	0.550	0.038	0.939	0.131
K1993	0.529	0.018	0.941	0.033	0.516	0.027	0.918	0.099
K1993	0.538	0.015	0.957	0.028	0.528	0.023	0.940	0.084
B0000	0.708	0.029	1.028	0.043	0.792	0.159	1.150	0.462
B1956-1	0.829	0.026	0.970	0.032	0.742	0.142	0.867	0.333
B1956-1	0.849	0.021	0.993	0.026	0.829	0.120	0.969	0.282
B1956-2	0.831	0.024	0.972	0.030	0.750	0.133	0.878	0.312
B1977	0.791	0.029	1.019	0.039	0.810	0.076	1.044	0.198
B1981	0.758	0.033	0.992	0.044	0.752	0.075	0.984	0.196
B1981	0.706	0.019	0.924	0.027	0.647	0.046	0.846	0.122
B1986	0.777	0.022	1.032	0.031	0.795	0.044	1.055	0.117
B1987	0.786	0.030	0.962	0.038	0.765	0.056	0.936	0.138
B1989-1	0.706	0.021	0.948	0.030	0.683	0.038	0.917	0.102
B1989-2	0.677	0.020	0.909	0.028	0.637	0.036	0.855	0.098
B1990	0.678	0.021	0.910	0.030	0.642	0.036	0.862	0.098
B1990	0.719	0.017	0.965	0.025	0.705	0.030	0.946	0.082
B1991	0.743	0.028	0.991	0.039	0.740	0.045	0.986	0.122

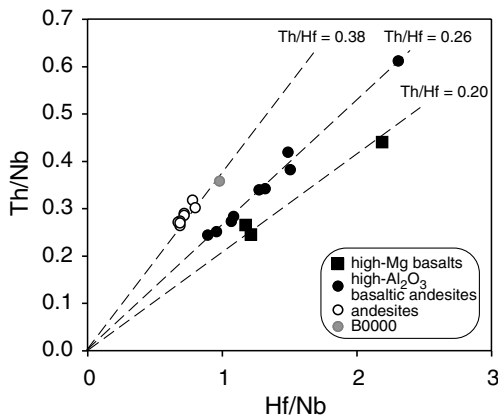


Fig. 5. Th/Nb versus Hf/Nb diagram showing that fluid-immobile, incompatible trace element ratios, such as Th/Hf, vary between the three lava groups but remain constant within group.

sional setting of the CKD. In this case, because dynamic melting also increases (²³⁰Th/²³²Th), the time lag since fluid addition could be slightly shorter (~100 kyr) and the 100 kyr DM line on Fig. 8a reflects the sum of fluid addition followed by 100 kyr of decay and then dynamic melting. Why this time lag should be so long in such an active system remains unresolved. Furthermore, the Ra excesses produced

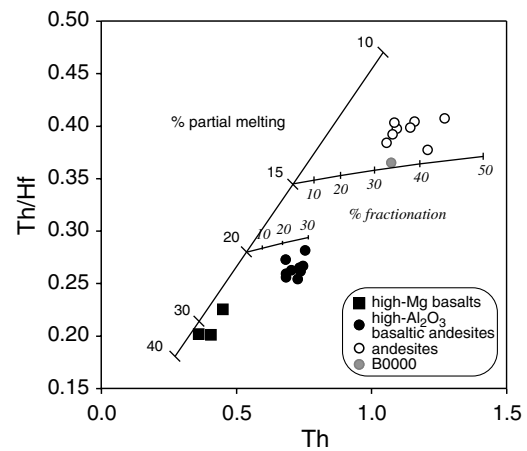


Fig. 6. Th/Hf versus Th process identification diagram showing that the three lava groups can be related to the same source if they represent increasing degrees of fractionation from parental magmas which reflected decreasing extents of partial melting. The batch partial melting model used partition coefficients from the 1.5 GPa MPY experiments of McDade et al. (2003) and assumed a mantle source which contained 0.11 ppm Th and 0.92 ppm Hf and was composed of 53% olivine, 25% orthopyroxene and 22% clinopyroxene. The fractionation model used partition coefficients compiled by Halliday et al. (1995) to simulate fractional crystallisation of an assemblage comprised of 50% olivine, 40% clinopyroxene, 5% orthopyroxene and 5% plagioclase.

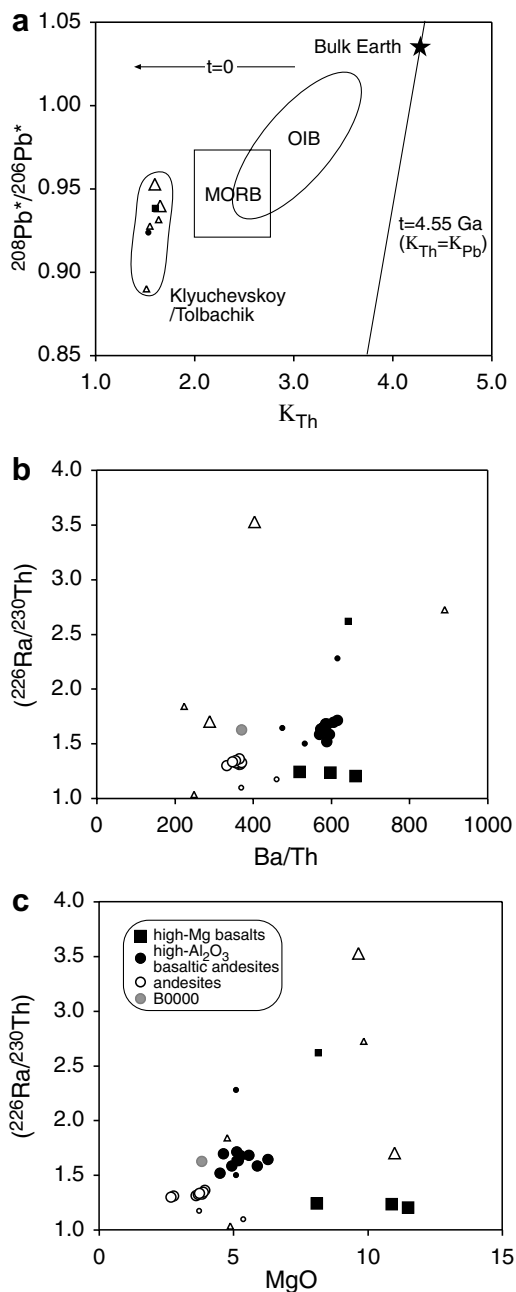


Fig. 7. (a) $^{208}\text{Pb}^*/^{206}\text{Pb}^*$ versus K_{Th} showing Klyuchevskoy and Tolbachik data from [Dosseto et al. \(2003\)](#) along with Tolbachik data from [Turner et al. \(1998\)](#) and [Dosseto et al. \(2003\)](#). (b) $(^{226}\text{Ra}/^{230}\text{Th})$ versus Ba/Th. (c) $(^{226}\text{Ra}/^{230}\text{Th})$ versus MgO. In (b) and (c) large symbols are data from this study for lavas from Klyuchevskoy and Bezmianny whereas large triangles are data for Tolbachik lavas from [Turner et al. \(1998\)](#). Small symbols are data for equivalent rock types from [Dosseto et al. \(2003\)](#).

by fluid addition will obviously have decayed during the elapsed 100 kyr before partial melting occurs (see [Fig. 8a](#)). However, in this regard we note that [Dorendorf et al. \(2000\)](#) similarly argued that fluid addition occurred prior to, and did not initiate, partial melting. In this model, partial melting occurs in response to decompression

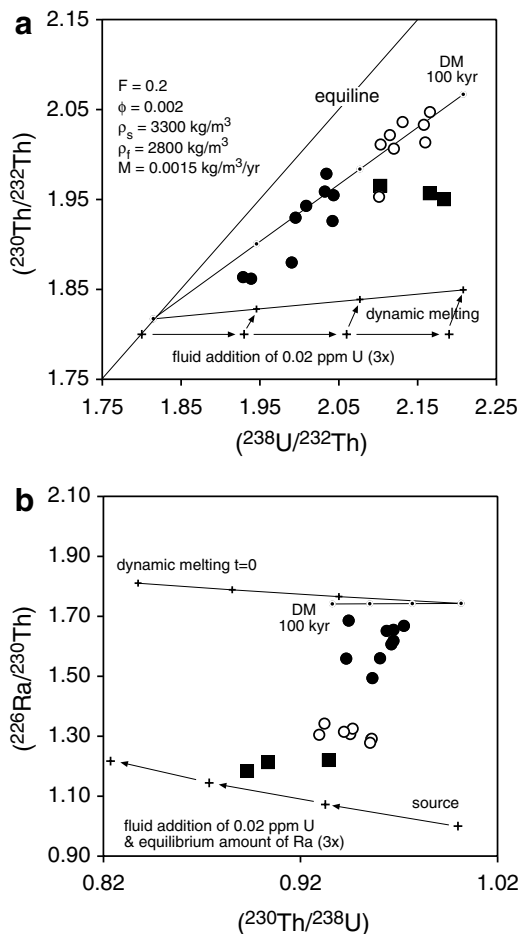


Fig. 8. Results of dynamic melting models using the formulation of [Williams and Gill \(1989\)](#). To simulate variable metasomatism of source initially in secular equilibrium with 277 ppb U and a $(^{230}\text{Th}/^{232}\text{Th})$ ratio of 1.8, three modified compositions were calculated assuming three increments of fluid addition containing 20 ppb U each. This is shown on (a) as the large crosses connected by arrows. Dynamic melting of the four resulting source compositions used 3 GPa partition coefficients from [Blundy and Wood \(2003\)](#), the source mineralogy from [Fig. 6](#) and is shown as the curve with small crosses. A second model, shown as the curve with dots, was identical excepting that fluid addition was assumed to have occurred 100 kyr prior to partial melting. For (b) the amount of ^{226}Ra added by each fluid increment was simply determined assuming secular equilibrium with 20 ppb U. Other parameters as listed in (a). Sample B0000 plots outside of the field of view in (a). Symbols as in previous Figures.

beneath Klyuchevskoy due to the active intra-arc rifting that is producing the Central Kamchatka Depression (cf. [Fig. 1](#)). The model Ra excesses, produced solely by partial melting at this time are broadly similar to the larger excesses observed in the high- Al_2O_3 basaltic andesites ([Fig. 8b](#)). The main difference between the zero age and 100 kyr models is the range in $(^{230}\text{Th}/^{238}\text{U})$ as the Ra excesses are dominated by partial melting, rather than fluid addition. If this is representative of a primary Ra signal, then the lower $(^{226}\text{Ra}/^{230}\text{Th})$ observed in the andesites

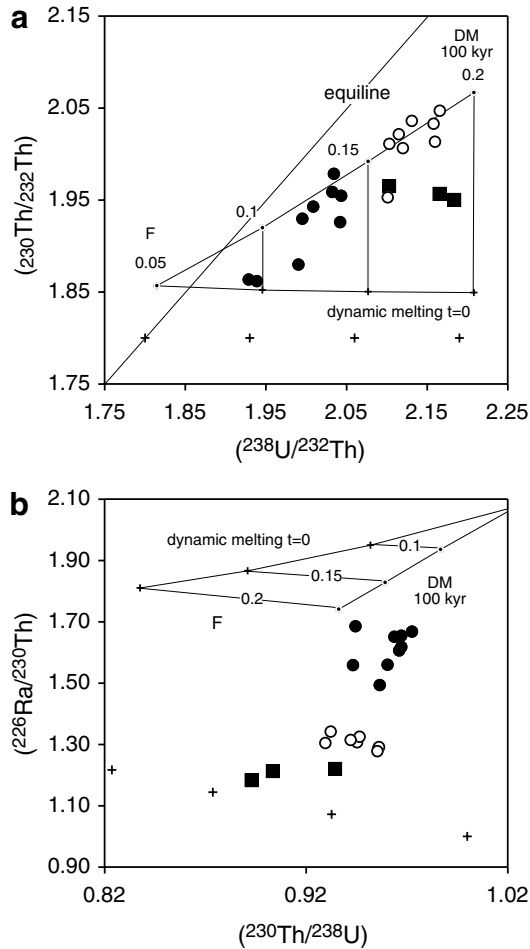


Fig. 9. Variant on the model shown on Fig. 8 whereby the extent of partial melting varies in proportion to the amount of fluid addition. Sample B0000 plots outside of the field of view in (a). Symbols as in previous Figures.

could reflect fractionation over a few 1000 yrs. However, such a model would imply that the high-MgO basalts had the longest crustal residence time of all the lavas, which is inconsistent with the evidence that these represent unmodified mantle melts.

Since our incompatible element modelling indicates each of the three magma suites reflecting differing extents of partial melting it is not unreasonable to infer that the extent of melting might increase with amount of fluid addition and also increasing source U/Th ratio. Thus, we also examine the effects of a coupled increase in the extent of melting, fluid addition and U/Th source ratio on U–Th–Ra disequilibria, keeping all other variables constant. Again, varying the total extent of partial melting has little effect upon U–Th disequilibria and so the broad conclusions there remain unchanged (Fig. 9). On the $(^{226}\text{Ra}/^{230}\text{Th})$ versus $(^{230}\text{Th}/^{238}\text{U})$ diagram, the result is to produce positive arrays (Fig. 9b). However, the model does not overlap the observed data and $(^{226}\text{Ra}/^{230}\text{Th})$ decreases with increasing total extent of melting which is the opposite of the inference from Fig. 6 that the extent of melting decreases from the

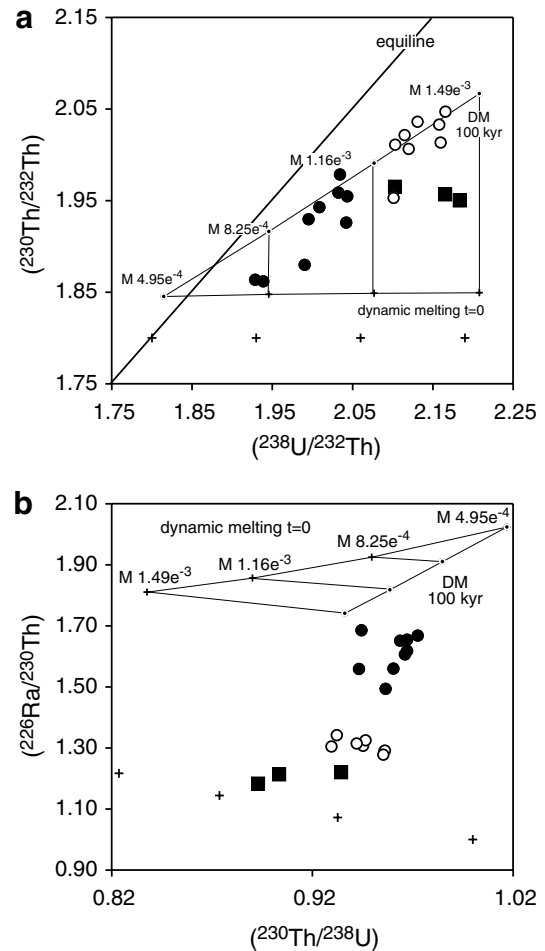


Fig. 10. Variant on the model shown on Fig. 8 whereby the rate of melting ($\text{kg}/\text{m}^3/\text{a}$) increases in proportion to the amount of fluid addition. Sample B0000 plots outside of the field of view in (a). Symbols as in previous Figures.

high-MgO basalts through the high- Al_2O_3 basaltic andesites to the andesites.

Another possibility is that the rate of melting increases with increasing fluid contribution, although melt productivity is predicted to decrease with fluid addition (Hirschmann et al., 1999). For completeness, Fig. 10 shows that results of a model in which the rate of melting was progressively faster for the sources with higher U/Th ratios. The results are very similar to the model used for Fig. 9 because, if all other variables remain constant, the effect of increasing the total extent of melting is equivalent to increasing the rate of melting. Thus, the problem remains that, for reasonable input parameters, the Ra excesses produced exceed those observed in all but the high- Al_2O_3 basaltic andesites implying longer residence times for the high-MgO basalts than the andesites which seems improbable.

The highly incompatible nature of Ra means that the extent of ^{226}Ra – ^{230}Th disequilibria is most strongly controlled by the residual porosity (ϕ) during melting. Thus, our final model investigates a scenario in which the residual porosity

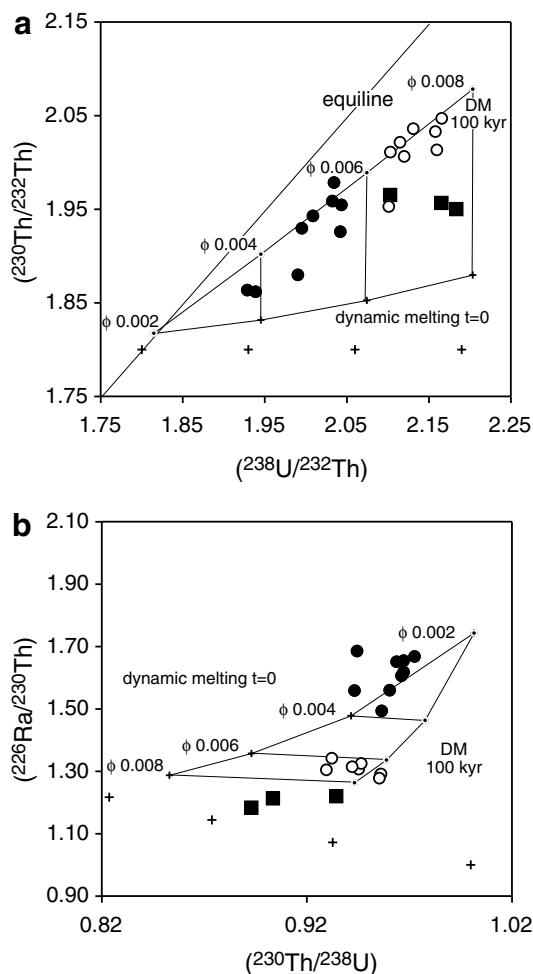


Fig. 11. Variant on the model shown on Fig. 8 whereby the threshold porosity in the melting region increases with the amount of fluid addition. Sample B0000 plots outside of the field of view in (a). Symbols as in previous figures.

increases in proportion to amount of fluid addition (i.e. with increasing U/Th ratio). The effect upon U–Th disequilibria is minimal since $(^{230}\text{Th}/^{238}\text{U})$ is most sensitive to the rate of melting (Fig. 11). However, $(^{226}\text{Ra}/^{230}\text{Th})$ decreases rapidly with increasing ϕ and this model encompasses the majority of the observed data. If correct, the implication is that the high-MgO basalts were extracted at higher ϕ than the andesites whereas the high- Al_2O_3 basaltic andesites were extracted at the lowest ϕ . If the total melt extent increases with the amount of fluid addition, the model can produce a slightly better fit to the data.

None of the models presented here are entirely satisfactory, mainly because the andesites plot between the high-MgO and high- Al_2O_3 basaltic andesites on the $(^{226}\text{Ra}/^{230}\text{Th})$ versus $(^{230}\text{Th}/^{238}\text{U})$ diagram. Nevertheless, the different forward melting models show that the Ra excesses could result primarily from partial melting and could be essentially unmodified in the erupted lavas (Fig. 11b). The implication is that the fractionation involved in producing the high- Al_2O_3 basaltic andesites and andesites (cf.

Fig. 6) occurred on a time scale less than the half-life of ^{226}Ra (1600 yrs).

5.3. ^{210}Pb systematics and implications for degassing at Klyuchevskoy and Bezyminny

^{210}Pb – ^{226}Ra disequilibria afford the opportunity to investigate processes involving migration of the gaseous intermediate nuclide, ^{222}Rn , relative to the melt phase in magmas (e.g. Gauthier and Condomines, 1999; Turner et al., 2004; Berlo et al., 2004; Reagan et al., 2006). The ^{210}Pb disequilibria data from Klyuchevskoy and Bezyminny are plotted against eruption year in Fig. 12. The initial $(^{210}\text{Pb}/^{226}\text{Ra})$ values for Klyuchevskoy's high-Mg basalts could not be adequately constrained because of low activities of both ^{210}Pb and ^{226}Ra , and because they all erupted more than 68 years before present, which is more than three times the half life of ^{210}Pb (22.6 yrs). The higher nuclide activities and relative youth of the basaltic andesites from Klyuchevskoy and andesites from Bezyminny allow for a better resolution of initial $(^{210}\text{Pb}/^{226}\text{Ra})$ values. These are nearly all within 2σ analytical error of secular equilibrium, demonstrating that differential losses or gains of ^{222}Rn by gas-melt movement in this highly active volcanic system are relatively restricted in magnitude or duration. These data also show that there is no systematic difference in $(^{210}\text{Pb}/^{226}\text{Ra})$ between the basaltic andesites of Klyuchevskoy and the andesites of Bezyminny (Fig. 12). However, one exception is the first high- Al_2O_3 basaltic andesite to erupt (K1945) that has an average $(^{210}\text{Pb}/^{226}\text{Ra})$ ratio of value of approximately 1.6. This is consistent with the hypothesis that the high- Al_2O_3 basalts represent a new batch of magma. Enrichments in ^{210}Pb over ^{226}Ra in magmas have been explained by fluxing of the magma by a ^{222}Rn -rich gas derived either from a large volume of magma and/or local wallrocks and groundwaters (Reagan et al., 2006; Berlo et al., 2006). The lack of significant ^{210}Pb excesses after 1946 suggests that only the top of the rising body of basaltic andesite had a significant and persistent ^{222}Rn excess, or that it acquired excess ^{210}Pb . The latter explanation is inconsistent with Pb/Th values in this sample, which are lower than for younger basaltic andesites. Therefore, we

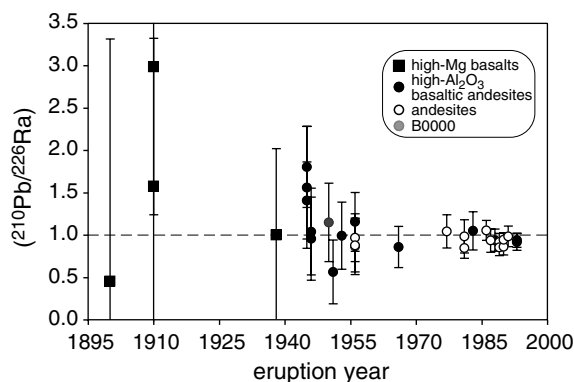


Fig. 12. $(^{210}\text{Pb}/^{226}\text{Ra})$ versus eruption year. All multiple analyses from Table 3 are plotted and the error bars are 2σ . Dashed line indicates secular equilibrium.

propose that ^{222}Rn derived from a much larger volume of magma (see Reagan et al., 2006; Berlo et al., 2006) or from heated wall-rocks and pore fluids fluxed through this basaltic andesite but not through underlying magmas. This probably occurred as this new basaltic andesite rose into the shallow conduit system previously occupied by high-Mg basalts, which is similar to the circumstance at Arenal Volcano, where only the first erupted lava with in-mixed “recharge magma” had a ^{210}Pb excess (Reagan et al., 2006). The only other sample with disequilibria outside of analytical uncertainty is a high- Al_2O_3 basaltic andesite (K1951) has a ^{210}Pb deficit just outside of analytical uncertainty and, for this sample, the degassing model of Gauthier and Condomines (1999) would indicate ~ 13 years of continuous degassing, assuming completely efficient removal of ^{222}Rn and no magma recharge. However, this time scale is difficult to reconcile with the observation that magma erupted 6 years earlier was in equilibrium and so we are reluctant to assign much significance to this measurement since the sample is almost within 2σ error of secular equilibrium.

6. CONCLUSIONS

One of the major challenges of this study was to explain why the most primitive rocks (high-MgO basalts) have high Ba/Th and larger ^{238}U excesses, but smaller ^{226}Ra excesses, than associated lavas. These characteristics are atypical of arc lavas and may indicate that, in some circumstances, ^{226}Ra excesses can reflect partial melting rather than fluid addition. Despite all being erupted within the same century from the same volcanic centre, the three lava groups from Klyuchevskoy and Bezymianny appear to come from three different magma batches and liquid lines of descent. Modelling suggests that there may be a link between the extent of partial melting in their mantle source region and the subsequent degree of fractionation as the magmas ascend through the crust. This fractionation is likely to have occurred on timescales significantly less than 1000 years if observed ^{226}Ra excesses largely reflect variable residual porosity in the melting column. Forward models suggest that those portions of the source that had undergone the greatest addition of U by fluids from the subducting plate also underwent the greatest extents of partial melting at the highest residual porosity. At Klyuchevskoy, a change from eruption of high-MgO to high- Al_2O_3 basaltic andesites around 1945 is reflected in an increase in size of ^{226}Ra excess which seems to require a simultaneous decrease in residual porosity and suggests a rapid changes in the melting regime. The eruption of andesites at Bezymianny simultaneous with the eruption of basaltic andesites at Klyuchevskoy further suggests that different degree melts produced at differing residual porosity can be formed and extracted from the melt region at the same time. A major caveat is that different conclusions regarding the high- Al_2O_3 basalts and andesites would be reached if the high-MgO basalts from Tolbachik were assumed as parental melts. Thus, the melting processes beneath the region are demonstrably complex. They have clearly been influenced by both fluid addition from the subducting plate and extension and decompression beneath the Central Kamchatka

Depression. Finally, the ^{210}Pb data, which are mostly in equilibrium with ^{226}Ra , suggest that there was restricted relative magma-gas movement in this system.

ACKNOWLEDGEMENTS

We thank Alexei Ozerov for providing samples to K.W.W.S. and Tony Dosseto for helpful comments on the manuscript. This work also benefited significantly from constructive formal reviews by Mary Reid, Richard Arculus, and Jim Gill. This study used instrumentation funded by Australian Research Council LIEF and DEST Systemic Infrastructure Grants, Macquarie University and Industry. S.T. acknowledges the support of an Australian Research Council Federation Fellowship. K.W.W.S. acknowledges the support of NSF Grant EAR-0610671 and M.R. NSF Grants EAR 0504362 and EAR 0609670. This is GEMOC publication #488.

APPENDIX. U–TH–RA MEASUREMENTS AT WHOI

U and Th concentrations were measured by ID ICPMS using the ThermoFinnigan Element 2 and the activities of several short-lived isotopes were measured by γ -spectrometry. Vials with 10 gm of rock powder (grain size < 100 μm) were inserted into a closed-end coaxial well-type High Purity Germanium (HP-Ge) detector manufactured by CANBERRA shielded by lead and copper. The resolution of this detector is <3.0 keV at 1.33 MeV and <2.0 keV at 122 keV with $\sim 40\%$ relative efficiency. The outer diameter and length of the detector are 65 mm each while the diameter and depth of the well are 33 and 48 mm, respectively. This CANBERRA detector uses a single large fast plastic scintillation shield (80 cm \times 80 cm \times 5 cm, Bicron BC408 Newbury, Ohio, www.bicron.com <<http://www.bicron.com>>) above the gamma detector to reduce background counts from cosmic radiation. The delay of the signal from the fast plastic scintillator required to match the signal from the germanium crystal and the length of the timing window were determined by experiment to veto errant signals while not increasing the dead time of the detector. A Plexiglas glove box enclosure around the lead shielding filled with nitrogen boiled off from the dewar further reduced background counts by removing ambient radon.

The HP-Ge detector can measure gamma rays in the approximate range of 40–11,000 keV although the efficiency of the detector is linear only up to ~ 100 keV. For higher energy gamma rays, a correction is applied for detector sensitivity. For our study, gamma rays in the range of 40–950 keV were measured. A self-absorption correction, taking into account differences in density and chemical compositions of the rock powders is also routinely applied. This correction is only significant for the low-energy gamma rays (<300 keV), such as the 46.5 keV peak of ^{210}Pb (maximum 20%).

The activity of ^{226}Ra is determined from the 351.99 keV line of ^{214}Pb . The activity of ^{232}Th is determined through three different gamma lines: 338.4 and 911.07 keV of ^{228}Ac , and 583.14 of ^{208}Tl . The activities of the different nuclides are calculated by comparing the count rates (counts per hour per gram of sample) of a given peak for

the sample and standard. ATHO is used for a calibrating standard, assuming all its daughter nuclides from ^{230}Th on down to ^{206}Pb and ^{232}Th on down to ^{208}Pb are in secular equilibrium. For quality assurance we also measure USGS standards BCR2 and W2 as unknowns.

REFERENCES

- Allegre C. J. and Minster J. F. (1978) Quantitative models of trace element behaviour in magmatic processes. *Earth Planet. Sci. Lett.* **38**, 1–12.
- Ariskin A. A., Barmina G. S., Ozerov A. Y. and Nielsen R. L. (1995) Genesis of high-alumina basalts from Klyuchevskoy volcano. *Petrology* **3**, 496–521.
- Baranov B. V., Seliverstov N. I., Murav'ev A. V. and Muzurov E. L. (1991) The Komondorsky basin as a product of spreading behind a transform plate boundary. *Tectonophysics* **199**, 237–269.
- Berlo K., Blundy J., Turner S., Cashman K., Hawkesworth C. and Black S. (2004) Geochemical precursors to volcanic activity at Mount St. Helens, U.S.A.. *Science* **306**, 1167–1169.
- Berlo K., Turner S., Black S., Hawkesworth C. and Blundy J. (2006) Tracing magma degassing prior to eruption using ($^{210}\text{Pb}/^{226}\text{Ra}$) disequilibria in volcanic deposits of the 1980–1986 eruptions of Mount St Helens. *Earth Planet. Sci. Lett.* **249**, 337–349.
- Birck J. L. (1986) K, Rb, Sr isotopic analysis: application to Rb–Sr chronology. *Chem. Geol.* **56**, 73–83.
- Blundy, J., Wood, B., 2003. Mineral-melt partitioning of Uranium, Thorium and their daughters. In Uranium-series geochemistry (eds. B. Bourdon, G. M. Henderson, C. C. Lundstrom and S. P. Turner), *Rev. Mineral. Geochem.*, vol. 52, pp. 59–123.
- Bourdon B., Henderson G., Lundstrom C. and Turner S. (2003) Uranium series geochemistry. *Rev. Mineral. Geochem.* **52**, 656.
- Brophy J. G. and Marsh B. D. (1986) On the origin of high alumina arc basalt and the mechanics of melt extraction. *J. Petrol.* **27**, 763–789.
- Cheng H., Edwards R. L., Hoff J., Gallup C. D., Richards D. A. and Asmerom Y. (2000) The half lives of uranium-234 and thorium-230. *Chem. Geol.* **169**, 17–33.
- Crawford A. J., Falloon T. J. and Eggins S. (1987) The origin of island arc high-alumina basalts. *Contrib. Mineral. Petrol.* **97**, 417–430.
- Dorendorf F., Wiechert U. and Wörner G. (2000) Hydrated sub-arc mantle: a source for the Kluchevskoy volcano, Kamchatka/Russia. *Earth Planet. Sci. Lett.* **175**, 69–86.
- Dosseto A., Turner S. and Douglas G. B. (2006) Uranium-series isotopes in colloids and sediments: time scale for sediment production and transport in the Murray-Darling river system. *Earth Planet. Sci. Lett.* **246**, 418–431.
- Dosseto A., Bourdon B., Joron J. L. and Dupré B. (2003) U–Th–Pa–Ra study of the Kamchatka arc: new constraints on the genesis of arc lavas. *Geochim. Cosmochim. Acta* **67**, 2857–2877.
- Fedotov S. A., Khrenov A. P. and Jarinov N. A. (1987) Klyuchevskoy volcano, its activity 1932–1986 and possible development. *Volcanol. Seismol.* **4**, 3–16.
- Fournelle J. and Marsh B. D. (1991) Shishaldin volcano; Aleutian high-alumina basalts and the question of plagioclase accumulation. *Geology* **19**, 234–237.
- Gauthier P.-J. and Condomines M. (1999) ^{210}Pb – ^{226}Ra radioactive disequilibria in recent lavas and radon degassing: inferences on the magma chamber dynamics at Stromboli and Merapi volcanoes. *Earth Planet. Sci. Lett.* **172**, 111–126.
- Geist E. L., Vallier T. L. and Scholl D. W. (1994) Origin, transport, and emplacement of an exotic island-arc terrane exposed in eastern Kamchatka, Russia. *Geol. Soc. Am. Bull.* **106**, 1182–1194.
- Halliday A. N., Lee D.-C., Tommasini S., Davies G. R., Paslick C. R., Fitton J. G. and James D. E. (1995) Incompatible trace elements in OIB and MORB and source enrichment in the sub-oceanic mantle. *Earth Planet. Sci. Lett.* **133**, 379–395.
- Hawkesworth C., George R., Turner S. and Zellmer G. (2004) Timescales of magmatic processes. *Earth Planet. Sci. Lett.* **218**, 1–16.
- Hirschmann M. M., Asimow P. D., Ghiorso M. S. and Stolper E. M. (1999) Calculation of peridotite partial melting from thermodynamic models of minerals and melts. III Controls on isobaric melt production and the effect of water on melt production. *J. Petrol.* **40**, 831–851.
- Hochstaedter A. G., Kepezshinskas P. and Defant M. (1996) Insights into the volcanic arc mantle wedge from magneisan lavas from the Kamchatka arc. *J. Geophys. Res.* **101**, 697–712.
- Kelemen P. B. (1990) Reaction between ultramafic rock and fractionating basaltic magma: I. Phase relations, the origin of calc-alkaline magma series, and the formation of discordant dunite. *J. Petrol.* **31**, 51–98.
- Kepezshinskas P., McDermott F., Defant M. J., Hochstaedter A., Drummond M. S., Hawkesworth C. J., Koloskov A., Maury R. C. and Bellon H. (1997) Trace element and Sr–Nd–Pb isotopic constraints on a three-component model of Kamchatka arc petrogenesis. *Geochim. Cosmochim. Acta* **61**, 577–600.
- Kersting A. B. and Arculus R. J. (1994) Klyuchevskoy volcano, Kamchatka, Russia: the role of high-flux recharged, trapped, and fractionated magma chamber(s) in the genesis of high- Al_2O_3 from high-MgO basalt. *J. Petrol.* **35**, 1–41.
- Kersting A. B. and Arculus R. J. (1995) Pb isotope composition of Klyuchevskoy volcano, Kamchatka and North Pacific sediments: implications for magma genesis and crustal recycling in the Kamchatkan arc. *Earth Planet. Sci. Lett.* **136**, 133–148.
- Knaack, C., Cornelius, S., and Hooper, P.R., 1994. Trace Element Analysis of Rocks and Minerals by ICP-MS, Open File Report, Department of Geology, Washington State University.
- McDade P., Blundy J. D. and Wood B. J. (2003) Trace element partitioning on the Tinaquillo lherzolite solidus at 1.5 GPa. *Phys. Earth Planet. Inter.* **139**, 129–147.
- Nichols I. A. and Ringwood A. E. (1973) Effects of water on olivine stability in tholeiite and the production of silica-saturated magmas in the island-arc environment. *J. Geol.* **81**, 285–300.
- Ozerov A. Y. (2000) The evolution of high-alumina basalts of the Klyuchevskoy volcano, Kamchatka, Russia, based on microprobe analyses of mineral inclusions. *J. Volcanol. Geotherm. Res.* **95**, 65–79.
- Ozerov A. Y., Arishkin A. A., Kyle Ph., Bogoyavlenskaya G. E. and Karpenko S. F. (1997) Petrological–geochemical model for genetic relationships between basaltic and andesitic magmatism of Kluchevskoi and Bezymyanni volcanoes, Kamchatka. *Petrology* **5**, 550–569, translated from Russian.
- Peate D. W., Kokfelt T. F., Hawkesworth C. J., van Calsteren P. W., Hergt J. M. and Pearce J. A. (2001) U-series isotope data on Lau Basin glasses: the role of subduction related fluids during melt generation in back-arc basins. *J. Petrol.* **42**, 1449–1470.
- Reagan M., Tepley, III, F. J., Gill J. B., Wortel M. and Hartman B. (2005) Rapid time scales of basalt to andesite differentiation at Anatahan volcano, Mariana Islands. *J. Volcanol. Geotherm. Res.* **146**, 171–183.
- Reagan M. K., Tepley, III, F. J., Gill J. B., Wortel M. and Garrison J. (2006) Timescales of degassing and crystallization implied by ^{210}Po – ^{210}Pb – ^{226}Ra disequilibria for andesitic lavas erupted from Arenal volcano. *J. Volcanol. Geotherm. Res.* **157**, 135–146.

- Thomas R. B., Hirschmann M. M., Cheng H., Reagan M. K. and Edwards R. L. (2002) ($^{231}\text{Pa}/^{235}\text{U}$)–($^{230}\text{Th}/^{238}\text{U}$) of young mafic volcanic rocks from Nicaragua and Costa Rica and the influence of flux melting on U-series systematics of arc lavas. *Geochim. Cosmochim. Acta* **66**, 4287–4309.
- Turner S., McDermott F., Hawkesworth C. and Kepezhinskas P. (1998) A U-series study of lavas from Kamchatka and the Aleutians: constraints on source composition and melting processes. *Contrib. Mineral. Petrol.* **133**, 217–234.
- Turner S., Bourdon B., Hawkesworth C. and Evans P. (2000) ^{226}Ra – ^{230}Th evidence for multiple dehydration events, rapid melt ascent and the time scales of differentiation beneath the Tonga-Kermadec island arc. *Earth Planet. Sci. Lett.* **179**, 581–593.
- Turner, S., Bourdon, B., and Gill, J., 2003. Insights into magma genesis at convergent margins from U-series isotopes. In Uranium series geochemistry (eds. B. Bourdon, G. Henderson, C. Lundstrom, and S. Turner), *Rev. Mineral. Geochem.*, vol. 52, pp. 255–315.
- Turner S., Black S. and Berlo K. (2004) ^{210}Pb – ^{226}Ra and ^{232}Th – ^{228}Ra systematics in young arc lavas: implications for magma degassing and ascent rates. *Earth Planet. Sci. Lett.* **227**, 1–16.
- Turner S., Regelous M., Hawkesworth C. and Rostami K. (2006) Partial melting processes above subducting plates: constraints from ^{231}Pa – ^{235}U disequilibria. *Geochim. Cosmochim. Acta* **70**, 480–503.
- Williams R. W. and Gill J. B. (1989) Effects of partial melting on the uranium decay series. *Geochim. Cosmochim. Acta* **53**, 1607–1619.

Associate editor: Martin A. Menzies